



**HAL**  
open science

# Fast Antenna Array Diagnosis from a Small Number of Far-Field Measurements

Benjamin Fuchs, Laurent Le Coq, Marco Donald Migliore

► **To cite this version:**

Benjamin Fuchs, Laurent Le Coq, Marco Donald Migliore. Fast Antenna Array Diagnosis from a Small Number of Far-Field Measurements. IEEE Transactions on Antennas and Propagation, 2016, 64 (6), pp.2227–2235. 10.1109/TAP.2016.2547023 . hal-01343530

**HAL Id: hal-01343530**

**<https://univ-rennes.hal.science/hal-01343530>**

Submitted on 21 Jan 2021

**HAL** is a multi-disciplinary open access archive for the deposit and dissemination of scientific research documents, whether they are published or not. The documents may come from teaching and research institutions in France or abroad, or from public or private research centers.

L'archive ouverte pluridisciplinaire **HAL**, est destinée au dépôt et à la diffusion de documents scientifiques de niveau recherche, publiés ou non, émanant des établissements d'enseignement et de recherche français ou étrangers, des laboratoires publics ou privés.

# Fast Antenna Array Diagnosis from a Small Number of Far-Field Measurements

Benjamin Fuchs, *Member, IEEE*, Laurent Le Coq, and Marco Donald Migliore, *Member, IEEE*

**Abstract**—The fast diagnosis of antenna arrays from a small number of far-field measurements is addressed. With the a priori knowledge of the failure-free array radiation pattern, it is possible to reformulate the diagnosis problem such as only the faulty elements or the localized field differences have to be retrieved. Efficient and readily available sparse recovery algorithms can then be applied to identify the failures from a small number of measurements compared to standard diagnosis techniques, and hence speed up the diagnosis. More specifically, three regularization procedures namely the minimization of the  $\ell_1$ , Total Variation and the mixed  $\ell_1/\ell_2$  norm are used to solve the ill-posed array diagnosis problems. These approaches are compared to two standard fault identification techniques: the back-propagation algorithm and the matrix inversion method for the diagnosis from simulated and measured data. The simulation of a  $10 \times 10$  waveguide array in realistic conditions of noise and taking into account the potential scaling factor between two measurements is first presented. Then, a reflectarray composed of 193 cells with metallic strips to emulate phase failures is considered. Both numerical and experimental results confirm the effectiveness of the sparse recovery algorithms and the importance of prior information on the source.

**Index Terms**—Antenna measurements, Arrays, compressive sensing.

## I. INTRODUCTION

The identification of failures in large antenna arrays is a theoretically and practically relevant topic with important applications both for civilian and military market. Indeed, many existing and upcoming technologies require the use of sophisticated phased or active arrays with a large number of elements. One can cite the large arrays used in modern RADAR systems, the massive MIMO and full MIMO systems that are currently under development [1], [2] and the huge development of personal communication devices that calls for the design of always more complex antenna arrays. Consequently, there is and will be an important need for the fast testing and diagnosis of these complex antenna systems.

A powerful method for array testing is based on far-field measurements. The acquired data are successively elaborated to identify possible failures in the radiating elements of the Antenna Under Test (AUT). A commonly used technique is the back-propagation algorithm (BPA) [3]. The BPA can be applied to planar arrays and is based on the Fourier relationship between the radiated far-field and the field on the array aperture. A generalization of the BPA is the Matrix

Method Algorithm (MMA) [4], [5]. The MMA is based on standard tools of linear algebra to stabilize the inversion of the matrix relating the field on the array aperture to the radiated far-field.

Both the BPA and the MMA requires a large number of measurements, and consequently a long measurement time in case of arrays with a large number of elements. One way to overcome this drawback is to use the a priori knowledge of a failure-free array radiation pattern so that only the faulty array elements have to be identified. The use of a differential scenario combined with sparse recovery algorithms has been applied in [6]–[11] to retrieve the element excitations and perform the array diagnosis. This approach leads to a small number of unknowns, but it requires a detailed model of the array and an accurate knowledge of the radiating element patterns to provide relevant results.

In this paper, the problem is not considered at the element excitation level but the distribution of the field on the array aperture is estimated. It allows to identify the modifications of the field aperture distribution due to phenomena that cannot be modelled as simple element failures, such as the diffraction contributions from the edges of the array or the multiple reflections between the reflectarray and its feed. The price to pay to get a more complete information on the AUT is the number of unknowns that is then much larger. However, for sparse recovery based approaches, the number of required measurements slowly increases (in a logarithmical way) with the number of unknowns [12]–[14]. Therefore, the strategy of field reconstruction takes fully advantage of the main key feature of sparse based techniques.

The so-formulated diagnosis problem can be solved using readily available routines whose computation times are slightly higher than those of standard approaches. It is important to point out that the overall time taken to achieve the antenna diagnosis depends mostly on the measurement time, the post-processing time being several order of magnitude faster. This is why the proposed sparse recovery approaches, that require a small number of measurements, enable a fast antenna diagnosis.

Three different strategies based on sparse recovery to perform antenna diagnostic are presented in this paper. More specifically, the minimization of the  $\ell_1$  norm, the Total Variation (TV) norm, and the mixed  $\ell_1/\ell_2$  norm are used as regularizers to solve the inverse problem. It is then possible to derive, from the fields reconstructed on the array aperture, a proper array diagnosis. These methods are first applied to the far-field simulated data of a 100 elements array. The diagnosis performances are assessed and compared to two

Manuscript received xx, 2015; revised xx, xx.

B. Fuchs and L. Le Coq are with the IETR / University of Rennes I, France. (e-mail: {benjamin.fuchs;laurent.le-coq}@univ-rennes1.fr). M.D. Migliore is with the DIEI, University of Cassino e Lazio Meridionale, Italy. (e-mail mdmiglio@unicas.it).

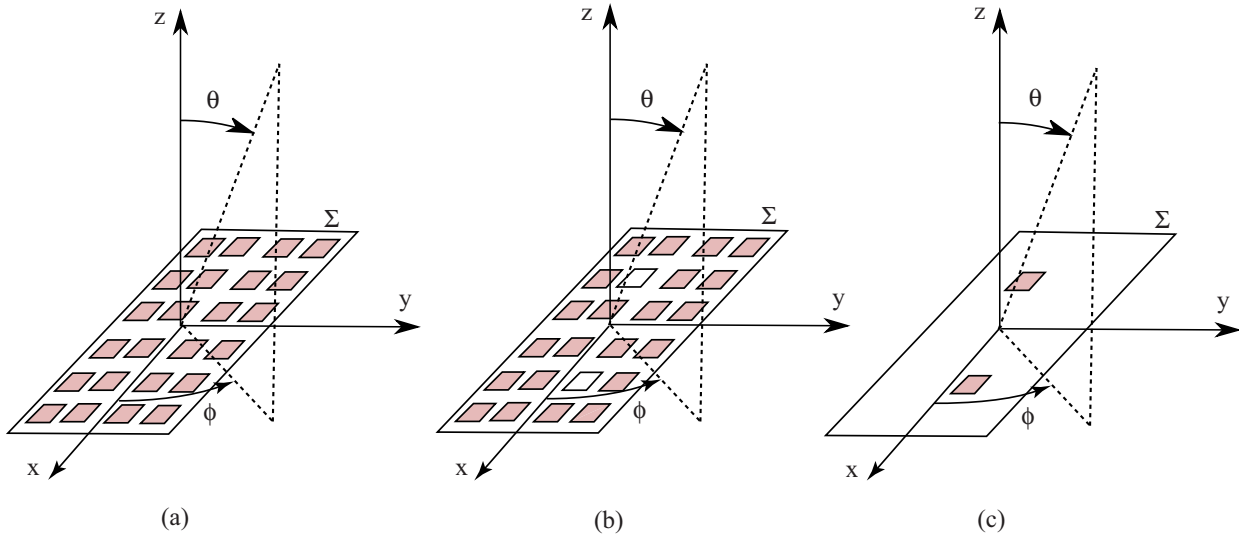


Fig. 1. Array and reference system. (a) Reference Antenna without failures (RA) or *golden array*. (b) Antenna Under Test (AUT). (c) Differential Antenna (DA). In this representation, the number of failures is  $S = 2$  and the total number of elements is  $N = 24$ .

standard fault identification techniques (the BPA and MMA algorithms) in various realistic conditions. Then, the proposed approaches are applied to the measured the far-field data of a reflectarray antenna in which failures have been added on purpose. This antenna has already been used [10], [11] to analyze the performance of the  $\ell_1$  minimization algorithm. Here, new regularization schemes are introduced and applied at the electric field distribution level to further improve the antenna diagnosis as confirmed by the comparisons with BPA and MMA techniques. Though applied on planar radiating structures, the proposed procedure can be used to perform the diagnostic of any type of arrays including conformal ones.

## II. THE PROBLEM OF ARRAY DIAGNOSIS

### A. Differential Setup

Let us consider a planar array radiating in free space. The field radiated by the array is measured (in amplitude and phase) in the far-field zone. This array, represented in Fig. 1(b) is called the Antenna Under Test (AUT). The quantities related to the AUT are denoted by the superscript 'd'. In particular,  $\mathbf{E}^d(x, y)$  is the tangential field on the array aperture, i.e.  $\mathbf{E}^d(x, y) = E_x^d(x, y)\hat{x} + E_y^d(x, y)\hat{y}$ , wherein  $E_x^d(x, y)$  and  $E_y^d(x, y)$  are respectively the  $x$  and  $y$  components of the electric field on  $\Sigma$ . The far-field  $\mathbf{F}^d(r, \theta, \phi)$  is the field measured on a portion of an hemispherical surface ( $0 \leq \theta \leq \pi/2$ ,  $0 \leq \phi \leq 2\pi$ ) at a distance  $r$  from the phase center of the AUT, such as  $r > 2D^2/\lambda$  where  $D$  is the maximum dimension of the antenna and  $\lambda$  is the free space wavelength.

We assume that the far-field (amplitude and phase) of a *golden array* represented in Fig. 1(a), i.e. an array without failures, is available. This array is the *Reference Antenna* (RA) and the quantities related to the RA are denoted by the superscript 'r'. In particular,  $\mathbf{E}^r(x, y)$  is the field on the RA aperture  $\Sigma$  and  $\mathbf{F}^r(r, \theta, \phi)$  is the radiated far-field.

The *Differential Antenna* (DA) is represented in Fig. 1(c). Its tangential field distribution  $\mathbf{E}(x, y)$  on  $\Sigma$  is equal to the

difference between the RA and AUT distributions, and its far-field  $\mathbf{F}(r, \theta, \phi)$  is given by the difference between the RA and AUT far-field:

$$\mathbf{E}(x, y) = \mathbf{E}^r(x, y) - \mathbf{E}^d(x, y) \quad (1)$$

$$\mathbf{F}(r, \theta, \phi) = \mathbf{F}^r(r, \theta, \phi) - \mathbf{F}^d(r, \theta, \phi) \quad (2)$$

The use of this differential setup allows to have an equivalent problem in which only the area corresponding to a field modification (due to failures) radiates. A visual inspection of the field distribution on the DA allows the identification of the problems affecting the AUT.

### B. Conventional diagnosis approaches

A widely adopted method to identify the failures is the back-propagation algorithm (BPA). The BPA is based on the Fourier relationship between the tangential components of the field distribution on the DA surface  $\mathbf{E}(x, y)$  and the far-field  $\mathbf{F}(r, \theta, \phi)$  radiated by the DA. As well known, the spatial resolution on the array aperture is practically limited to  $\lambda/2$ . A smaller number of unknowns would lead to an undersampling of the tangential field distribution on the aperture. Thus, in case of an array of dimensions  $2a \times 2b$ , the minimum number of unknowns is  $N \simeq ab/\lambda^2$ . A larger number of unknowns does not increase the accuracy of the reconstruction, but acts as an oversampling of a band-limited function which leads to an interpolation of the data.

Another method proposed to identify the failures of large antenna arrays is the matrix method algorithm (MMA). The MMA is based on the linear relationship between the vectors  $\mathbf{x} \in C^N$  and  $\mathbf{y} \in C^M$  collecting the sampled values of  $\mathbf{E}(x, y)$  and  $\mathbf{F}(k_x, k_y)$  respectively, wherein  $k_x = k_0 \sin(\theta) \cos(\phi)$ ,  $k_y = k_0 \sin(\theta) \sin(\phi)$ ,  $k_0 = 2\pi/\lambda$ . The linear operator is modeled by the radiation matrix  $\mathbf{A}$  which leads to:

$$\mathbf{y} = \mathbf{A}\mathbf{x}. \quad (3)$$

The matrix  $\mathbf{A}$  is, in general, ill-conditioned and regularization methods are required to restore the stability of the solution [15]. A common approach, used in this paper, is the truncated Singular Value Decomposition (SVD) [16], [17].

### C. On the number of measurement points

Both the BPA and MMA techniques require a large number of measurements. In a differential setup, we can reasonably assume that the field on the DA is localized which means that the unknown to be retrieved is highly sparse as schematized in Fig. 1(c). In general, there is indeed a small number of failures  $S$  compared to the total number of radiating elements  $N$ , or similarly the field differences between the RA and the AUT are localized. The use of sparse recovery approaches allows the estimation of  $\mathbf{x}$  from a number of measurements significantly smaller than the one required by standard inversion approaches. A rigorous analysis in terms of information content of the electromagnetic field [17], [18] shows that the amount of information is reduced from  $O(N)$  to  $O(S \log N/S)$ , wherein  $O(\cdot)$  is the Landau symbol. Accordingly, it is at least theoretically possible to obtain a similar reduction in the number of data.

## III. RESOLUTION VIA COMPRESSED SENSING / SPARSE RECOVERY BASED APPROACHES

A standard approach for matrix inversion regularization is to introduce a priori information in the inversion. An effective method to achieve this regularization is to minimize an appropriately chosen norm  $p$  of the solution vector  $\mathbf{x}$ . The optimization problem to solve is then:

$$\min_{\mathbf{x}} \|\mathbf{x}\|_p \text{ subject to } \|\mathbf{y} - \mathbf{A}\mathbf{x}\|_2 \leq \epsilon \quad (4)$$

where  $\|\cdot\|_p$  stands for the  $\ell_p$  norm, and  $\epsilon$  depends on the noise and uncertainties affecting the data.

It is important to note that there are many readily available routines to solve efficiently convex optimization problems such as (4), e.g. [19], [20].

Three different norms  $\ell_p$ , chosen according to the a priori information about the differential setup of the diagnosis problem, are now described to regularize the inversion. They are applied in Section IV and V to perform the diagnostic of simulated and measured radiating structures respectively.

### A. $\ell_1$ -norm

As previously discussed, it is reasonable to suppose that the solution  $\mathbf{x}$  is sparse. Consequently, the search space can be drastically reduced by introducing this a priori information in the inversion. In particular, the  $\ell_1$ -norm ( $\|\mathbf{x}\|_1 = \sum_k |x_k|$ ) is the best convex surrogate of the proper measure of the sparsity of a vector, i.e. the quasi-norm  $\ell_0$  that counts the number of non-zero occurrences of a vector. Consequently, the use of  $\ell_1$  norm in the inversion scheme (4) is an effective strategy to promote sparse solution [12], [21]. The so-regularized inversion problem is:

$$\min_{\mathbf{x}} \|\mathbf{x}\|_1 \text{ subject to } \|\mathbf{y} - \mathbf{A}\mathbf{x}\|_2 \leq \epsilon. \quad (5)$$

Let us point out that minimizing the  $\ell_1$ -norm enforces the sparsity of the solution point-wise, i.e. for each sample  $x_k$  of the field on the DA.

### B. Total Variation norm

We know a priori that our solution  $\mathbf{x}$  has a few discontinuities that are due to the presence of the failures. Apart from these failures, the field  $\mathbf{x}$  is expected to be flat and close to zero. Thus, the use of the Total Variation norm (TV-norm) is a good candidate to regularize  $\mathbf{X}$ . The TV-norm is indeed a smoothing function introduced in [22]. By minimizing the TV-norm of a matrix, we minimize its gradient, hence the smoothing effect. For 2D complex data  $\mathbf{X} \in \mathbb{C}^{M \times N}$ , the TV-norm reads:

$$\begin{aligned} \|\mathbf{X}\|_{\text{TV}} &= \sum_{m,n} |\mathbf{X}_{m+1,n} - \mathbf{X}_{m,n}| + |\mathbf{X}_{m,n+1} - \mathbf{X}_{m,n}| \quad (6) \\ &= \|\text{vec}(\nabla_x \mathbf{X})\|_1 + \|\text{vec}(\mathbf{X} \nabla_y)\|_1 \end{aligned}$$

where  $\text{vec}(\mathbf{X})$  produces a vector of length  $MN$  that contains the columns of  $\mathbf{X}$ , stacked below each other. The discrete gradient matrices  $\nabla_x$  and  $\nabla_y$  are of size  $M \times M$  and  $N \times N$  respectively, and equal to:

$$\nabla_x = \begin{bmatrix} -1 & 1 & & 0 \\ & \ddots & \ddots & \\ 0 & & -1 & 1 \end{bmatrix} \text{ and } \nabla_y = \begin{bmatrix} -1 & & & 0 \\ 1 & \ddots & & \\ & \ddots & \ddots & -1 \\ 0 & & & 1 \end{bmatrix}.$$

The optimization problem (4) becomes:

$$\min_{\mathbf{X}} \|\mathbf{X}\|_{\text{TV}} \text{ subject to } \|\mathbf{y} - \mathbf{A}\text{vec}(\mathbf{X})\|_2 \leq \epsilon. \quad (7)$$

### C. Mixed $\ell_1/\ell_2$ -norm

We can also take advantage of the knowledge about the structure of the problem at hand, specifically the position and dimensions of the radiating apertures. The solution vector  $\mathbf{x}$  is then divided into  $G$  groups  $\mathbf{x}^g$  corresponding to each radiating aperture  $g$ . Indeed, when one radiating element is faulty, then all discretization points  $x_k^g$  included in this radiating aperture should be faulty, i.e. non zero.

Let us divide the vector  $\mathbf{x}$  of length  $MN$  into  $G$  non overlapping groups denoted  $\mathbf{x}^g$  of size  $N_g$  such as  $\sum_{g=1}^G N_g = MN$ . The mixed  $\ell_1/\ell_2$ -norm is:

$$\|\mathbf{x}\|_{1,2} = \sum_{g=1}^G \|\mathbf{x}^g\|_2 = \sum_{g=1}^G \sqrt{|x_1^g|^2 + \dots + |x_{N_g}^g|^2}. \quad (8)$$

It behaves like an  $\ell_1$ -norm on the vector  $[\|\mathbf{x}^1\|_2, \dots, \|\mathbf{x}^g\|_2, \dots, \|\mathbf{x}^G\|_2]$  and therefore it induces group sparsity, in this case the sparsity at a radiating aperture level. A thorough description of group (also called structured) sparsity-inducing norms is given in [23]. The regularized inversion problem is then:

$$\min_{\mathbf{x}} \|\mathbf{x}\|_{1,2} \text{ subject to } \|\mathbf{y} - \mathbf{A}\mathbf{x}\|_2 \leq \epsilon. \quad (9)$$

## IV. NUMERICAL SIMULATIONS

### A. Settings

1) *Full Wave Simulation Setup*: Let us consider an array composed of  $10 \times 10$  WR90 open ended waveguides working at 10GHz as represented in Fig. 2. These waveguides of aperture size  $22.86 \times 10.16 \text{ mm}^2$  are uniformly spaced by  $\lambda$  and  $\lambda/2$  in the  $x$  and  $y$  directions respectively. The radiation pattern of this array has been computed with the full wave 3D electromagnetic software Ansys HFSS v.15.

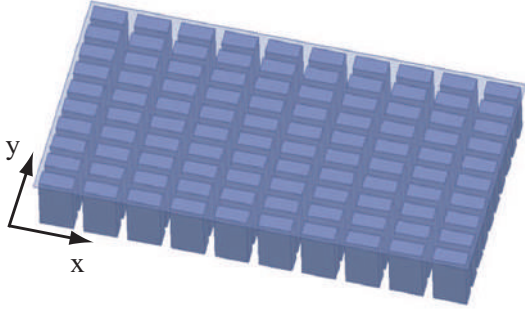


Fig. 2. Illustration of the 100 open-ended waveguide array simulated with HFSS for diagnostic purposes.

First, all  $N$  waveguides are fed with the same excitation value in order to emulate a failure-free array, i.e. the RA. Then,  $K$  failures in either amplitude  $\delta_A$  or phase  $\delta_\Phi$  are added so as to model the AUT.

2) *Noise*: In practice, measurements are contaminated by noise, therefore a Gaussian noise  $\mathbf{n}$  is added on both patterns of reference and with defaults as follows:  $\mathbf{y}_n^q = \mathbf{y}^q + \mathbf{n}^q$  with  $q = \{r, d\}$ . The level of the noise is determined by the Signal-to-Noise Ratio (SNR) that is defined from the maximum received field magnitude in order to fit with the dynamic range measurement. The noise is equal to:

$$\mathbf{n}^q = \frac{\mathcal{N}(0, 1) + j\mathcal{N}(0, 1)}{\sqrt{2}} \cdot \max|\mathbf{y}^q| \cdot 10^{-\text{SNR}_{dB}/20}.$$

where  $\mathcal{N}(0, 1)$  is a gaussian random vector of mean 0 and standard deviation 1.

The far-field considered in the inversion is then:  $\mathbf{y}_n = \mathbf{y}_n^r - \mathbf{y}_n^d$  and the problem (4) becomes:

$$\min_{\mathbf{x}} \|\mathbf{x}\|_p \text{ subject to } \|\mathbf{y}_n - \mathbf{A}\mathbf{x}\|_2 \leq \epsilon. \quad (10)$$

3) *Measurement Scaling Factor*: One practical problem in measurements is that there can be a complex scaling factor  $\gamma$  between the measurement of the AUT and the one of the RA:  $\mathbf{y}^d = \gamma\mathbf{y}^r$ . This scaling factor is also present if the RA data are available from simulation instead of measurement. Therefore, it is of interest to suppose that the differential far-field is:

$$\mathbf{y} = \gamma\mathbf{y}^r - \mathbf{y}^d \quad (11)$$

where  $\gamma$  is the unknown complex scalar that simulates the inevitable scaling (not due to element failures) in both amplitude and phase between the measurements  $\mathbf{y}^r$  and  $\mathbf{y}^d$ .

The unknown scaling in amplitude  $|\gamma|$  can be overcome by

normalizing both  $\mathbf{y}^r$  and  $\mathbf{y}^d$  with respect to the total radiated power  $\|\mathbf{y}^r\|_2$  and  $\|\mathbf{y}^d\|_2$  respectively. The small number of failures should indeed not impact in a significant way the total amount of radiated power. To compensate the scaling in phase  $\angle\gamma$ , we compute the global phase shift difference  $\Delta\Phi$  between  $\mathbf{y}^r$  and  $\mathbf{y}^d$  as follows:

$$\Delta\Phi = \frac{1}{M} \sum_{m=1}^M (\angle y_m^r - \angle y_m^d).$$

### B. Recovery Performances

In order to quantify the diagnostic performances let us introduce the following indicator. We first sum up the magnitudes of the field samples  $x_k$  included on each radiating aperture  $g$ :  $\alpha_g = \sum_k |x_k^g|$ , for  $g = 1, \dots, G$ . By doing so, we get a positive number per radiating element  $g$  from which we compute the difference  $\Delta_{FA}$  between the level of the lowest failure and highest false alarm. The value of  $\Delta_{FA}$  gives the margin to set a threshold to discriminate true failures from false alarms as represented in Fig. 3. The higher the margin  $\Delta_{FA}$  is, the easier the diagnostic is. A negative  $\Delta_{FA}$  means that the diagnostic is not correctly performed since a false alarm is then higher than a failure.

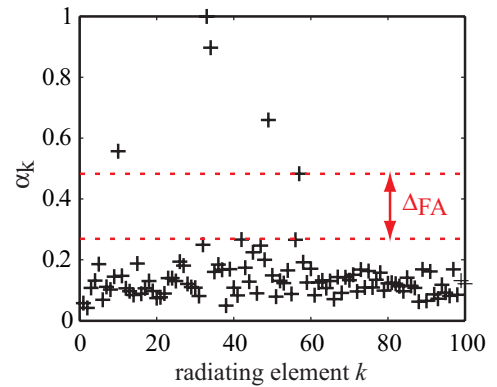


Fig. 3. Illustration of an array diagnostic result: the values  $\alpha_k$  are the level per radiating element  $k$  and the distance  $\Delta_{FA}$  is the margin between the lowest of the 5 errors (all assumed to be correct here) and the highest false alarm.

### C. Results

For each configuration, the simulation is repeated 100 times with a Gaussian white noise. All presented results are average values over these 100 simulations in order to get meaningful results. The following number of far-field data is considered to ensure the best possible reconstruction in all investigated configurations of noise and errors:  $2^5 = 1024$  for the BPA,  $30 \times 30 = 900$  for the MMA and  $12 \times 12 = 144$  for the sparse recovery based approaches. Whereas choosing a higher number of points do not improve the recovery, a reduced number of data could be employed in a few specific cases involving important errors and a high SNR.

The parameter  $\epsilon$  in the data fitting constraint of the sparse based approaches (4) is chosen to be higher than the noise level. We typically set  $\epsilon$  to be equal to  $1.1\|\mathbf{n}\|_2$ . In the case of

TABLE I

WAVEGUIDE ARRAY DIAGNOSTIC RESULTS -  $K=5$  AMPLITUDE ERRORS

Config.	SNR [dB]	Method	$\Delta_{FA}$
$\delta_A=1$	60	BPA	0.44
		MMA	0.54
		$\ell_1$ min	0.59
		TV. min	0.53
		$\ell_1/\ell_2$ min	0.79
	40	BPA	0.40
		MMA	0.47
		$\ell_1$ min	0.44
		TV. min	0.14
		$\ell_1/\ell_2$ min	0.67
$\delta_A=0.1$	100	BPA	0.45
		MMA	0.54
		$\ell_1$ min	0.59
		TV. min	0.45
		$\ell_1/\ell_2$ min	0.72
	60	BPA	0.33
		MMA	0.34
		$\ell_1$ min	0.21
		TV. min	0.00
		$\ell_1/\ell_2$ min	0.70

TABLE II

WAVEGUIDE ARRAY DIAGNOSTIC RESULTS -  $K=5$  PHASE ERRORS

Config.	SNR [dB]	Method	$\Delta_{FA}$
$\delta_\Phi=60^\circ$	60	BPA	0.56
		MMA	0.55
		$\ell_1$ min	0.65
		TV. min	0.47
		$\ell_1/\ell_2$ min	0.81
	40	BPA	0.50
		MMA	0.45
		$\ell_1$ min	0.45
		TV. min	0.10
		$\ell_1/\ell_2$ min	0.64
$\delta_\Phi=10^\circ$	100	BPA	0.57
		MMA	0.56
		$\ell_1$ min	0.62
		TV. min	0.44
		$\ell_1/\ell_2$ min	0.85
	60	BPA	0.55
		MMA	0.51
		$\ell_1$ min	0.59
		TV. min	0.38
		$\ell_1/\ell_2$ min	0.78

measurements, an estimation of the SNR is used to determine  $\epsilon$ . Our anechoic chamber exhibits a SNR of about 60 dB and the value of  $\epsilon$  is set accordingly.

An example of reconstruction results is given in Fig. 4. They illustrate the particularities of each inversion approach, namely the point-wise sparsity of the  $\ell_1$  minimization with visible localized ‘hot spots’ (Fig. 4(c)), the flat regions produced by the TV-norm minimization (Fig. 4(d)) and the group-wise sparsity provided by the  $\ell_1/\ell_2$  minimization in which the shape of the waveguide apertures are clearly reconstructed (Fig. 4(e)).

1) *Amplitude Failures:* We consider that  $K = 5$  waveguides are fed with an amplitude of  $1-\delta_A$  instead of 1 in order to simulate failures in amplitude. To assess the recovery, we compute the margin  $\Delta_{FA}$  for various SNR. The results are reported in Table I.

As expected, it is easier to perform the diagnostic when the error in amplitude is more important. Generally speaking, for the same SNR,  $\Delta_{FA}$  is greater when  $\delta_A = 1$  than for  $\delta_A = 0.1$ . The diagnostic result obtained by BPA, MMA and  $\ell_1$  minimization are quite similar. The diagnostic is not correct when the SNR is lower than 40 and 60 dB for an amplitude error  $\delta_A$  of 1 and 0.1 respectively. Let us point out that thanks to the a priori sparsity knowledge, the  $\ell_1$  minimization requires significantly less measurement points than the BPA and MMA as already discussed and shown in [6], [10], [11]. The TV-norm works less well than the other approaches when the SNR decreases, this is probably because the noise smooths the contrast required for a proper diagnostic. The highest  $\Delta_{FA}$ , i.e. the best diagnostic performances, are obtained when applying  $\ell_1/\ell_2$ -norm minimization, that uses stronger a priori information compared to the other compressive sensing based techniques.

2) *Phase Failures:* We consider that  $K = 5$  waveguides are fed with an amplitude of  $e^{j\delta_\Phi}$  instead of 1 in order to simulate failures in phase. To assess the recovery, we compute

the margin  $\Delta_{FA}$  for various SNR. The results are reported in Table II.

The comments made for amplitude failures hold in the case of phase failures. As we must expect, a large phase error  $\delta_\Phi=60^\circ$  is easier to diagnose than a small one  $\delta_\Phi=10^\circ$ . In addition, the diagnostic is not correct when the SNR is lower than 40 and 60 dB for a phase error  $\delta_\Phi$  of  $60^\circ$  and  $10^\circ$  respectively. The best diagnostic results are also obtained when using the group-sparsity regularizer.

3) *Scaling Factor:* We investigate the effect of the scaling factor and the efficiency of the compensation procedure described in Section IV-A.3. For that purpose, let us consider the BPA inversion technique and the case of  $K = 5$  failures with various SNR. We set a complex scaling factor  $\alpha$  of random amplitude between 0 and 10 and random phase between 0 and  $2\pi$ .

The diagnostic results (average value over 100 iterations) without and with compensation procedure are reported in Table III as well as the estimation of the phase shift error  $|\angle\alpha - \angle\hat{\alpha}|$ . Without compensation, the diagnostic always fails since  $\Delta_{FA} < 0$  for all investigated configurations. We observe that the compensation procedure helps significantly to improve the diagnostic. Of course, the diagnostic results are less good than in absence of scaling. We also note that the phase shift due to the scaling is fairly well estimated in case of important errors ( $\delta_A = 1$  and  $\delta_\Phi=60^\circ$ ) and very well approximated in case of small failures ( $\delta_A = 0.1$  and  $\delta_\Phi=5^\circ$ ) because the induced phase shift between  $\mathbf{y}_n^r$  and  $\mathbf{y}_n^d$  is then small. In conclusion, the proposed compensation approach turns out to be efficient but a calibration (if possible) between the measurements of  $\mathbf{y}^r$  and  $\mathbf{y}^d$  remains important to improve the quality of the diagnostic.

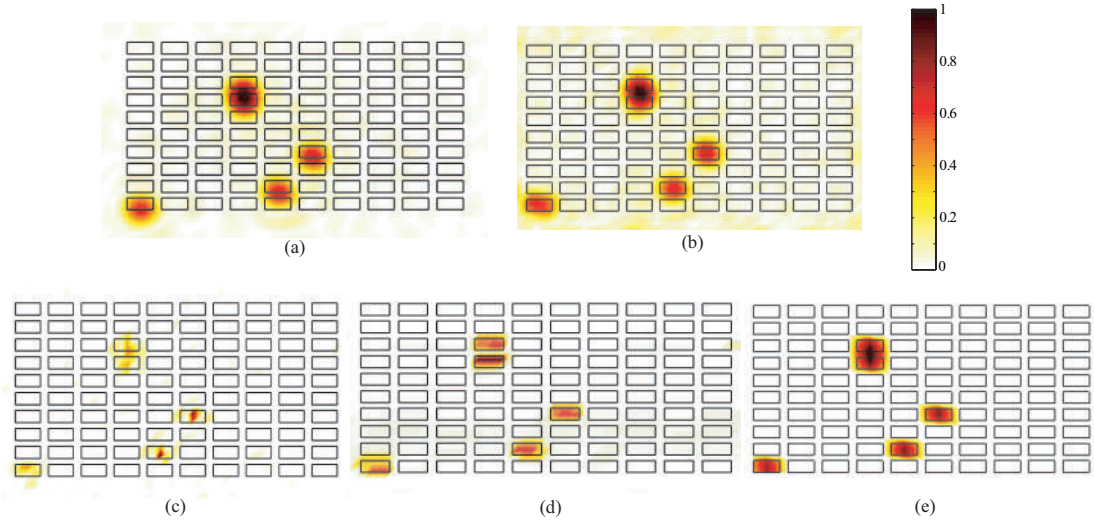


Fig. 4. Reconstructed excitation errors for the case of  $K = 5$  amplitude failures with  $\delta_A = 1$  and  $\text{SNR}=60$  dB obtained by: (a) BPA, (b) MMA, (c)  $\ell_1$ -norm minimization, (d) TV-norm minimization and (e)  $\ell_1/\ell_2$ -norm minimization.

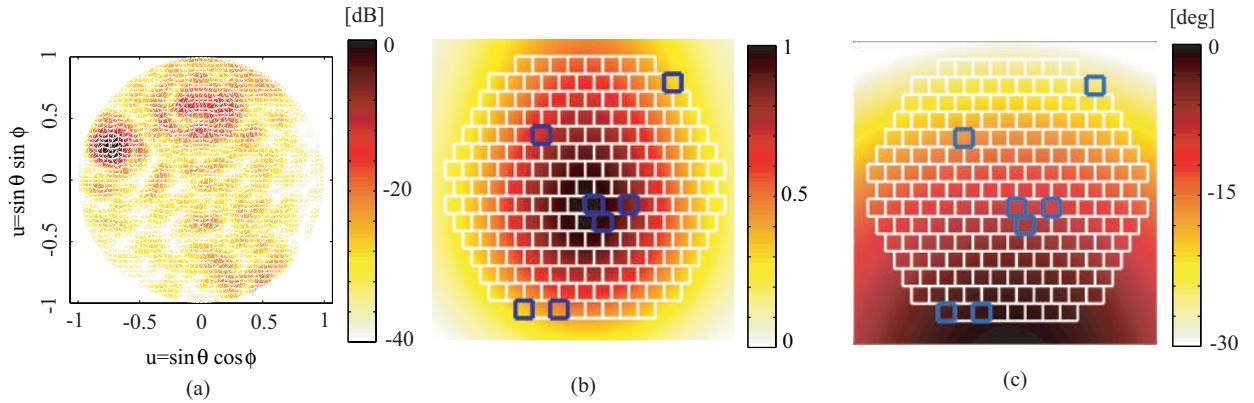


Fig. 5. (a) Normalized measured far-field radiated by the reflectarray without default at 12 GHz. Normalized (b) amplitude and (c) phase apodisation on the reflectarray due to the horn.

## V. EXPERIMENTAL RESULTS

### A. Measurement Settings

The proposed diagnostic approaches are now applied to measured data. The AUT is a reflectarray of 193 cells, re-radiating a beam tilted in both planes as shown in Fig. 5(a). This antenna has been designed by Thales Alenia Space in the framework of the project R3MEMS. A total number of 5536 co-polar and cross-polar data have been measured on a far-field half-sphere at 12 GHz.

Seven radiating elements have been covered by metallic square patches in order to emulate a phase failure on the element, as shown in Fig. 6. The so-induced phase errors are also reported in this figure.

The reflectarray is illuminated by a directive horn which causes a non uniform illumination of the cells as shown in Fig. 5(b,c). The horn apodisation is compensated before performing the inversion.

From the above data, the failures can be divided into three groups: two ‘important’ failures with a large phase difference and a strong horn illumination (specifically the failures hav-

ing phase difference equal to  $100^\circ$  and  $114^\circ$ ), two ‘medium’ failure with large phase difference but low illumination (the failure having phase difference equal to  $102^\circ$  and  $-143^\circ$ ) and three ‘less’ important failures, with small phase difference or medium phase difference but low amplitude illuminations (i.e. the failure with  $72^\circ$ ,  $23^\circ$ ,  $14^\circ$  phase difference).

### B. Reconstruction Results

As a first step, the MMA method is applied using a large number of measured data collected on a grid that is as close as possible to a  $30 \times 30$  uniformly spaced grid in the spectral domain. The results, obtained using these 900 measurement points, are plotted in Fig. 7(b). The two ‘important’ failures and one ‘medium’ failure are clearly visible. This result is the best field amplitude that can be reconstructed, and an increase of the number of measurement points does not lead to any improvement. Some variations in the aperture field amplitude can be noticed in other parts of the reflectarray. The BPA method is also applied using these 900 measurement points in order to check these results. The aperture field distribution,

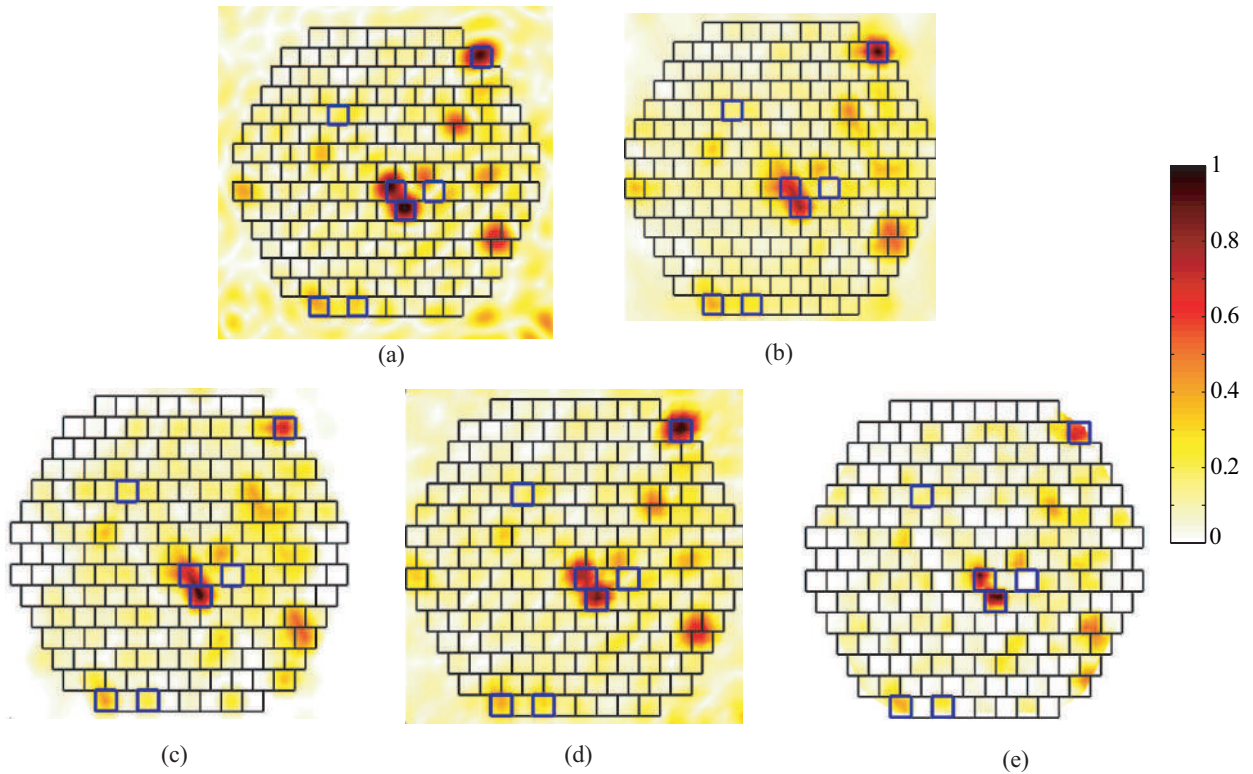


Fig. 7. Reconstructed field on the aperture of the reflectarray obtained by: (a) BPA from  $2^5 = 1024$  measurement points; (b) MMA from  $30 \times 30 = 900$  measurement points; and the sparse recovery based approaches from  $12 \times 12 = 144$  measurements points: (c)  $\ell_1$ -norm minimization, (d) TV-norm minimization, (e)  $\ell_1/\ell_2$ -norm minimization.

TABLE III  
INFLUENCE OF THE SCALING COMPENSATION -  $K=5$  FAILURES

config.	SNR [dB]	no compensation		with compensation	
		$\Delta_{FA}$	$\Delta_{FA}$	$ \angle\alpha - \angle\hat{\alpha} $ [deg]	
$\delta_A = 1$	100	-0.74	0.28	17.7	
	60	-0.72	0.27	17.9	
	40	-0.76	0.14	24.2	
$\delta_A = 0.1$	100	-0.29	0.46	0.2	
	60	-0.29	-0.03	2.4	
	40	-0.33	-0.46	16.7	
$\delta_\Phi = 60^\circ$	100	-0.19	0.23	17.0	
	60	-0.19	0.24	16.9	
	40	-0.21	0.01	24.4	
$\delta_\Phi = 5^\circ$	100	-0.22	0.23	1.7	
	60	-0.22	-0.04	3.0	
	40	-0.25	-0.42	18.3	

shown in Fig 7(a), confirms the general observation obtained using the MMA. Notably, the presence of similar field difference in areas wherein artificial failures were not imposed should be pointed out. Similar field mappings are obtained with the three proposed compressive sensing based inversion techniques using only  $12 \times 12 = 144$  measurement points, as shown in Fig. 7(c,d,e).

### C. Number of Measurement Points

The number of measurement points impact the quality of the field reconstruction and hence the diagnostic. In Fig. 8,

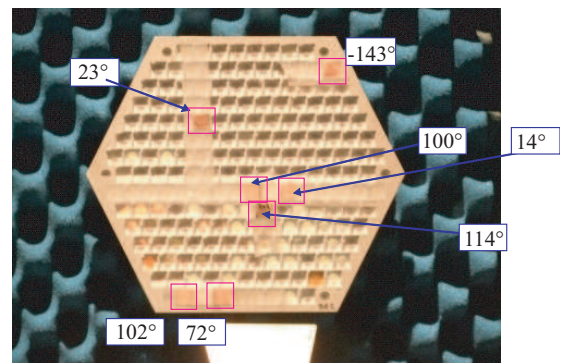


Fig. 6. Picture of the reflectarray with metallic strips to create 7 faulty elements. The induced phase errors are reported.

the fields reconstructed on the aperture of the reflectarray by the MMA and the three compressive sensing based approaches are compared in case of only  $9 \times 9 = 81$  and  $8 \times 8 = 64$  measurements. It appears clearly that the MMA manages to retrieve only the two main failures whereas the three proposed approaches are able to image the three main ones. The proposed techniques behave well in spite of a significant reduction of measurement data because of the added information on the sparsity of the solution or the derivative of the solution for the TV-norm minimization which helps the inversion procedure. The calculations are done on a 2.8GHz-CPU 8.0Go-RAM Xeon x64 and the computation times are also reported in this

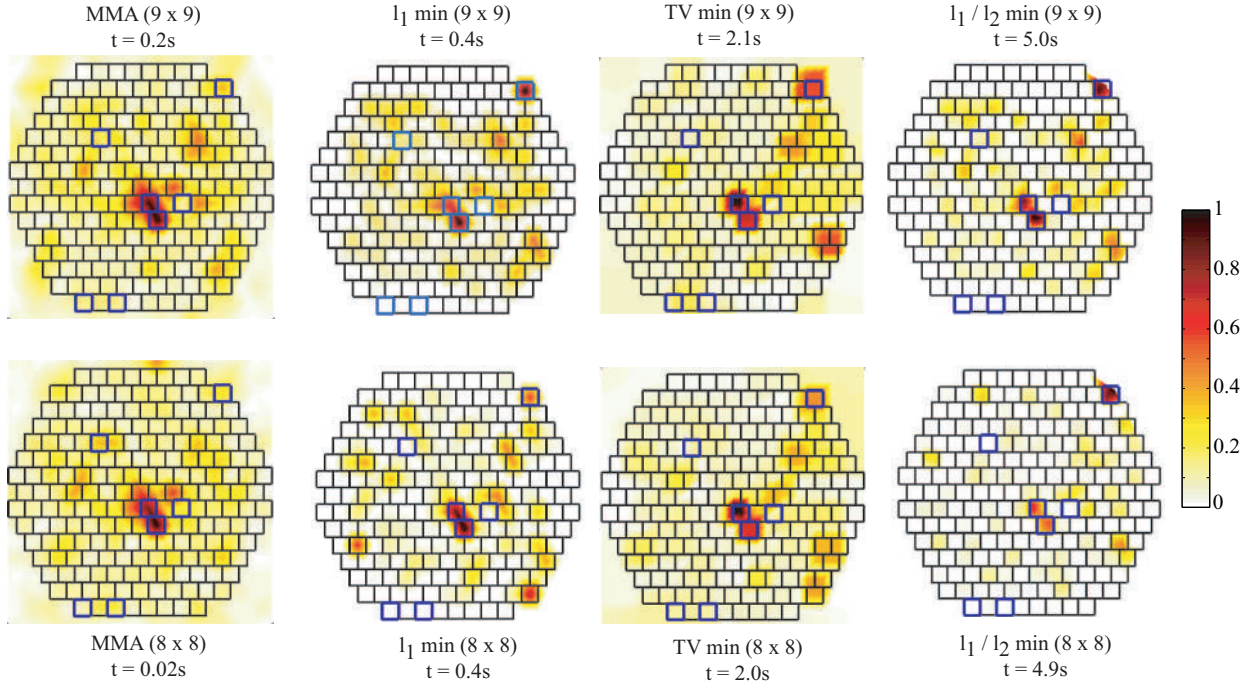


Fig. 8. Reconstructed field on the aperture of the reflectarray obtained from  $9 \times 9$  and  $8 \times 8$  measurement points using the MMA,  $\ell_1$ -norm minimization, TV-norm minimization,  $\ell_1/\ell_2$ -norm minimization with the associated computation times.

figure. Although the three proposed approaches are more time consuming than the MMA, this increase remains very small with respect to the measurement time cost.

Among the three sparse recovery techniques, the  $\ell_1/\ell_2$  norm minimization is the one that leads to the best mapping results. In this specific case, a priori information on the structure of the sparsity, specifically the geometry of the cells, are also added which is not the case for the  $\ell_1$  and TV norm minimization. This extra information further reduces the optimization space and thereby eases the inversion from a smaller number of measurement points.

## VI. CONCLUSION

Three methods for array diagnosis based on sparse recovery have been discussed and tested on simulated and measured antenna arrays. The results confirm that the proposed approaches allow to significantly decrease the number of measurements required for the diagnosis compared to two standard techniques: the Back-Propagation and the Matrix Method algorithms. For these antenna diagnosis procedures, the post-processing time (at most a few seconds) is negligible compared to the measurement time. Therefore, the proposed techniques that only calls for readily available routines, enable a faster antenna diagnosis compared to standard approaches. Both numerical and experimental results show that the mixed  $\ell_1/\ell_2$  norm minimization approach gives the best performance in terms of identification of radiating elements using a small set of data. This regularizer is indeed the one that uses the most a priori information about the radiating structure and specifically the positions of the reflectarray cells in order to define the groups of field samples.

The proposed approaches have been applied to perform the diagnosis of planar radiating structures but they can be straightforwardly extended to conformal antennas. Moreover, other types of unknown can be employed. The formulation using the electric field on the aperture can, for instance, be replaced by equivalent currents.

Finally, although many papers deal with sparse recovery algorithms in electromagnetism including array diagnosis procedures [24], only few of them report experimental data which are, in the end, the ground truth to test any procedure.

## ACKNOWLEDGMENT

This work was supported in part by the European Science Foundation (RNP NEWFOCUS). The authors want to thank Thalès Alenia Space for providing the reflectarray developed during the project R3MEMS.

## REFERENCES

- [1] 5G vision white paper, available at <http://www.samsung.com/global/business-images/insights/2015/Samsung-5G-Vision-0.pdf>, DMC R&D Center, Samsung Electronics Co., Ltd., February 2015.
- [2] 5G: A technological Vision, available at <http://www.huawei.com/5gwhitepaper/>, HUAWEI white paper, Huawei Technologies Co., Shenzhen.
- [3] J.J. Lee, E.M. Ferrer, D.P. Woollen, K.M. Lee, "Near-field probe used as a diagnostic tool to locate defective elements in an array antenna," *IEEE Trans. Antennas Propag.*, vol. 36, no. 3, pp.884-889, June 1988.
- [4] L. Gattoufi, D. Picard, Rekiouak, and J.C. Bolomey, "Matrix method for near-field diagnostic techniques of phased array antennas," *Proc. IEEE Int. Symp. Phased Array Systems and Technology*, pp.52-57 1996.
- [5] O.M. Bucci, M.D. Migliore, G. Panariello, G. Sgambato, "Accurate Diagnosis of Conformal Arrays from Near-Field data using the Matrix Method," *IEEE Trans. Antennas Propag.*, vol. 53, no. 3, pp. 1114-1120, March 2005.

- [6] M.D. Migliore, "A Compressed Sensing Approach for Array Diagnosis from a Small Set of Near-Field Measurements," *IEEE Trans. Antennas Propag.*, vol. 59, no. 6, pp. 2127-2133, June 2011.
- [7] G. Oliveri, P. Rocca, A. Massa, "Reliable Diagnosis of Large Linear Arrays, A Bayesian Compressive Sensing Approach," *IEEE Trans. Antennas Propag.*, vol. 60 no. 10, pp. 4627-4636, Oct. 2012.
- [8] M.D. Migliore, "Array Diagnosis From Far-Field Data Using the Theory of Random Partial Fourier Matrices," *IEEE Trans. on Antennas Wireless and Propagation Letters*, vol. 12, pp. 745-748, 2013.
- [9] B. Fuchs, M.D. Migliore, "Accurate Array Diagnosis from Near-Field Measurements Using  $\ell_1$  Reweighted Minimization," *IEEE Antennas and Propag. Symposium*, Orlando, 2013.
- [10] B. Fuchs, L. Le Coq, L. Ferro-Famil and M.D. Migliore, "Comparison of Methods for Reflectarray Diagnostic from Far Field Measurements," *IEEE International Symposium on Antennas and Propagation*, July 2015.
- [11] M.D. Migliore, B. Fuchs, L. Le Coq and L. Ferro-Famil, "Compressed Sensing Approach for Reflectarray Diagnostic from Far Field Measurements," *European Microwave Conference*, Sept. 2015.
- [12] D.L. Donoho, "Compressive Sensing," *IEEE Trans. on Information Theory*, vol. 52, no. 4, pp. 1289-1306, April 2006.
- [13] E.J. Candes, J. Romberg, T. Tao "Robust Uncertainty Principles: Exact Signal Reconstruction From Highly Incomplete Frequency Information," *IEEE Trans. on Inf. Theory*, vol. 52, no. 2, pp.489-509, Feb. 2006.
- [14] D. L. Donoho, J. Tanner, "Precise Undersampling Theorems," *Proc. of IEEE*, vol. 98, no. 6, pp. 913-923, June 2010.
- [15] G. Strang, "Introduction to Linear Algebra," Wellesley Cambridge Press, 4th edition, 2009.
- [16] O.M. Bucci, C.Gennarelli, C.Savarese, "Representation of Electromagnetic Fields over Arbitrary Surfaces by a Finite and non Redundant Number of Samples," *IEEE Trans. Antennas Propag.*, vol. 46, no. 3, pp. 351-359, March 1998.
- [17] M.D. Migliore, "On electromagnetics and information theory," *IEEE Trans. Antennas Propag.*, vol. 56, no. 10, pp. 3188-3200, Oct. 2008.
- [18] M.D. Migliore, "On the Sampling of the Electromagnetic Field Radiated by Sparse Sources," *IEEE Trans. Antennas Propag.*, vol. 63, no. 2, pp. 553-564, Feb. 2015.
- [19] YALL1 basic solver code: Y. Zhang, J. Yang, and W. Yin. YALL1: Your ALgorithms for L1, online at [yall1.blogs.rice.edu](http://yall1.blogs.rice.edu), 2011.
- [20] CVX Research, Inc. CVX: Matlab software for disciplined convex programming, version 2.0 beta. <http://cvxr.com/cvx>, September 2012.
- [21] E.J. Candès, M.B. Wakin and S.P. Boyd, "Enhancing sparsity by reweighted  $\ell_1$  minimization," *J. Fourier Analy. Appl.*, vol. 14, pp. 877-905, Dec. 2008.
- [22] L. Rudin, S. Osher, and E. Fatemi, "Nonlinear total variation based noise removal algorithms," *Physica D*, 60:259-68, 1992.
- [23] F. Bach, R. Jenatton, J. Mairal, G. Obozinski, "Optimization with sparsity-inducing penalties," *Foundations and Trends in Machine Learning*, vol.4, no. 1, pp. 1-106, 2012.
- [24] A. Massa, P. Rocca, and G. Oliveri, "Compressive Sensing in Electromagnetics - A Review," *IEEE Antennas and Propag. Magazine*, pp. 224-238, vol. 57, no. 1, Feb. 2015.



**Benjamin Fuchs** (S'06-M'08) received the M.Sc. and electrical engineering degrees in 2004 from the National Institute of Applied Science of Rennes, France. He received the Ph.D. degree in 2007 from the University of Rennes 1, France, and was during that period a visiting scholar at the University of Colorado at Boulder, USA. In 2009, he joined the Institute of Electronics and Telecommunications of Rennes (IETR) as a researcher at the Centre National de la Recherche Scientifique (CNRS). He has spent three years (2008 as postdoctoral research fellow and 2011-2012 on leave from CNRS) at the Swiss Federal Institute of Technology of Lausanne (EPFL) in Switzerland. His research interests include millimeter-wave antennas, focusing devices (lens antennas), array synthesis methods and inverse problems in electromagnetism.



**Laurent Le Coq** received the electronic engineering and radiocommunications degree and the french DEA degree (M.Sc.) in electronics in 1995 and the Ph. D. in 1999 from the National Institute of Applied Science (INSA), Rennes, France. In 1999, he joined IETR (Institute of Electronics and Telecommunications of Rennes), University of Rennes 1, as a research lab engineer, where he is responsible of the measurement technical facilities up to 110GHz, and of the prototyping service.

His activities in antenna measurements and development of related procedures involved him in more than 30 research contracts of national or european interest. He is author and co-author of more than 35 journal papers and 35 papers in conference proceedings.



**Marco Donald Migliore** (M'04) Marco Donald Migliore received the Laurea (Hons.) and Ph.D. degrees in electronic engineering from the University of Naples, Naples, Italy. He is an Associate Professor with the University of Cassino and Southern Lazio, Cassino, Italy, the director of the Microwave Laboratory and the Coordinator of the Information Engineering courses of the University of Cassino and Southern Lazio, He was a Visiting Professor with the University of San Diego in California, San Diego, CA, USA, and with the University of Rennes 1,

Rennes, France, and a Speaker with the Summer Research Lecture Series of the UCSD CALIT2 Advanced Network Science (ANS) in 2008. His research interests include the connections between electromagnetism and information theory, the analysis, synthesis, and characterization of antennas in complex environments, MIMO antennas and propagation, ad hoc wireless networks, antenna measurements, and energetic applications of microwaves. Prof. Migliore is a member of the Italian Electromagnetic Society (SIEM) and of the National Inter-University Consortium for Telecommunication (CNIT). He serves as a Referee for many scientific journals, including the *IEEE TRANSACTIONS ON ANTENNAS AND PROPAGATION*, the *IEEE ANTENNAS AND WIRELESS PROPAGATION LETTERS*, the *IEEE TRANSACTIONS ON VEHICULAR TECHNOLOGY*, the *Journal of Optical Society of America*, the *IEEE TRANSACTIONS ON SIGNAL PROCESSING* and the *IEEE TRANSACTIONS ON INFORMATION THEORY*.